JOURNAL OF MATERIALS SCIENCE **36** (2001) 321 – 327

Microstructure of (100) silicon wafer implanted by 1 MeV Ru^{+} ions

Y. L. CHEN*, G. SHAO
School of Mechanical and Materials Engineering, University of Surrey, Guildford, Surrey, GU2 5XH, England
E-mail: ylchen@liv.ac.uk

J. SHARPE, R. M. GWILLIAM, K. REESON KIRKBY, K. P. HOMEWOOD
School of Electronic Engineering, Information Technology and Mathematics, University of Surrey, Guildford, Surrey, GU2 5XH, England

M. J. GORINGE
School of Mechanical and Materials Engineering, University of Surrey, Guildford, Surrey, GU2 5XH, England

A p-type device grade silicon wafer was implanted by 1 MeV Ru^{+} ions to a dose of 5.67×10^{16} cm^{-2}. The microstructures of the as-implanted and annealed samples were studied mainly by analytical transmission electron microscopy (TEM) and X-ray diffraction (XRD). The results showed that the implantation resulted in a well-defined surface layer of about 910 nm in thickness. The layer was composed of ultra-fine Ru_2Si_3 crystallites in an amorphous matrix. After annealing, the inner part of the layer recovered completely to single crystal Si with nano-scaled Ru_2Si_3 embedded in it. A ∼660 nm thick polycrystalline region consisting of Si and Ru_2Si_3 grains was formed at the surface. © *2001 Kluwer Academic Publishers*

1. Introduction

There has been an enormous research effort on the synthesis of new semiconductors using techniques based on ion implantation and other deposition methods, due to increasing requirements by the semiconductor industry [1–5]. Among the emerging new materials, semiconducting silicides have attracted great attention and have been successfully synthesised in many Si based materials systems [3–6]. Initial results showed that Ru_2Si_3 is a potential candidate for optoelectronic applications [7–9]. Since Ru_2Si_3 was identified as a thermoelectric material [7], attempts have been made to fabricate the silicide and examine its electronic properties [8–10]. Henrion *et al.* produced Ru_2Si_3 film by a deposition and annealing route [8]. Both spectroscopic ellipsometry measurements and band structure calculation proved that Ru_2Si_3 is a semiconductor with a direct band gap. However, no microstructure of the film has been reported in their work. Lessen *et al.* synthesised Ru_2Si_3 by molecular beam epitaxy and the microstructure of the film was studied. However, they failed to prove whether the compound has semiconducting properties [9].

Ion beam synthesis (IBS) is a technique for the fabrication of thin films, which involves ion implantation and subsequent annealing at high temperatures [11]. The use of ion implantation is ubiquitous in the silicon semiconducting industry. Consequently, ion beam synthesis is a very attractive route for the production of silicon based materials with additional functionality that is compatible with existing ultra large scale integration (ULSI) technology. We have recently made the first effort to produce ruthenium silicide by IBS [12]. Optical measurements reported elsewhere confirmed that we have produced a new direct gap semiconductor in Si with a band gap of 0.9 ev corresponding to a wave length of 1.3 μm, which is compatible with optical fibre technology [12]. In this work, we shall report the microstructural development in the IBS Ru_2Si_3.

2. Experimental

Experiments were performed on a device grade p-type (100) Si wafer. Ru^{+} ions with an energy of 1 MeV were implanted into Si up to a dose of 5.67×10^{16} Ru^{+} cm^{-2}. During implantation the wafer was heated to a temperature of about 250 to 300°C by the incident beam. The implanted wafer was then cleaved into a number of smaller samples which were then analysed and/or annealed. Annealing was carried out in an 18-lamp optical furnace using a nitrogen ambient. A series of sequential isothermal annealing was undertaken over the temperature range from 100 to 1100°C. The annealing time was 1 hour at each temperature, increasing incrementally by 50°C on each occasion. Such an annealing route was used due to the difficulty in implanting Ru^{+}

* *Present Address:* Materials Science and Engineering, Department of Engineering, The University of Liverpool, Liverpool L69 3GH, UK.

in Si during this initial stage of our investigation. Microstructural investigation was performed on both the as-implanted material and the sample at the end of the final annealing at 1100°C.

The X-ray diffraction (XRD) experiments were carried out using a Philips PW 1050 X-ray diffractometer using the Cu K_α radiation. A transmission electron microscopy (TEM) study was conducted on a Philiphs CM200 microscope which is equipped with a Link^{ISI} 300 energy dispersive X-ray (EDX) spectroscopy system. Cross-sectional TEM (XTEM) samples were prepared by conventional techniques involving ion beam thinning as the final step.

3. Results and discussion

3.1. As-implanted samples

Fig. 1a is a representative XTEM bright field (BF) image of the as-implanted sample. It exhibits a well defined implanted layer of about 910 nm in thickness, on the surface of the Si substrate. Fig. 1b is a corresponding selected-area electron diffraction pattern (SADP) from the implanted layer. The diffused diffraction ring is due to the presence of an amorphous phase. The sharp crystalline diffraction ring corresponds to the lattice spacing of the (001) plane of the orthorhombic Ru_2Si_3 phase (Pearson structure symbol oP40, space group Pbcn, $a = 1.1057$ nm, $b = 0.8934$ nm and $c = 0.5533$ nm).

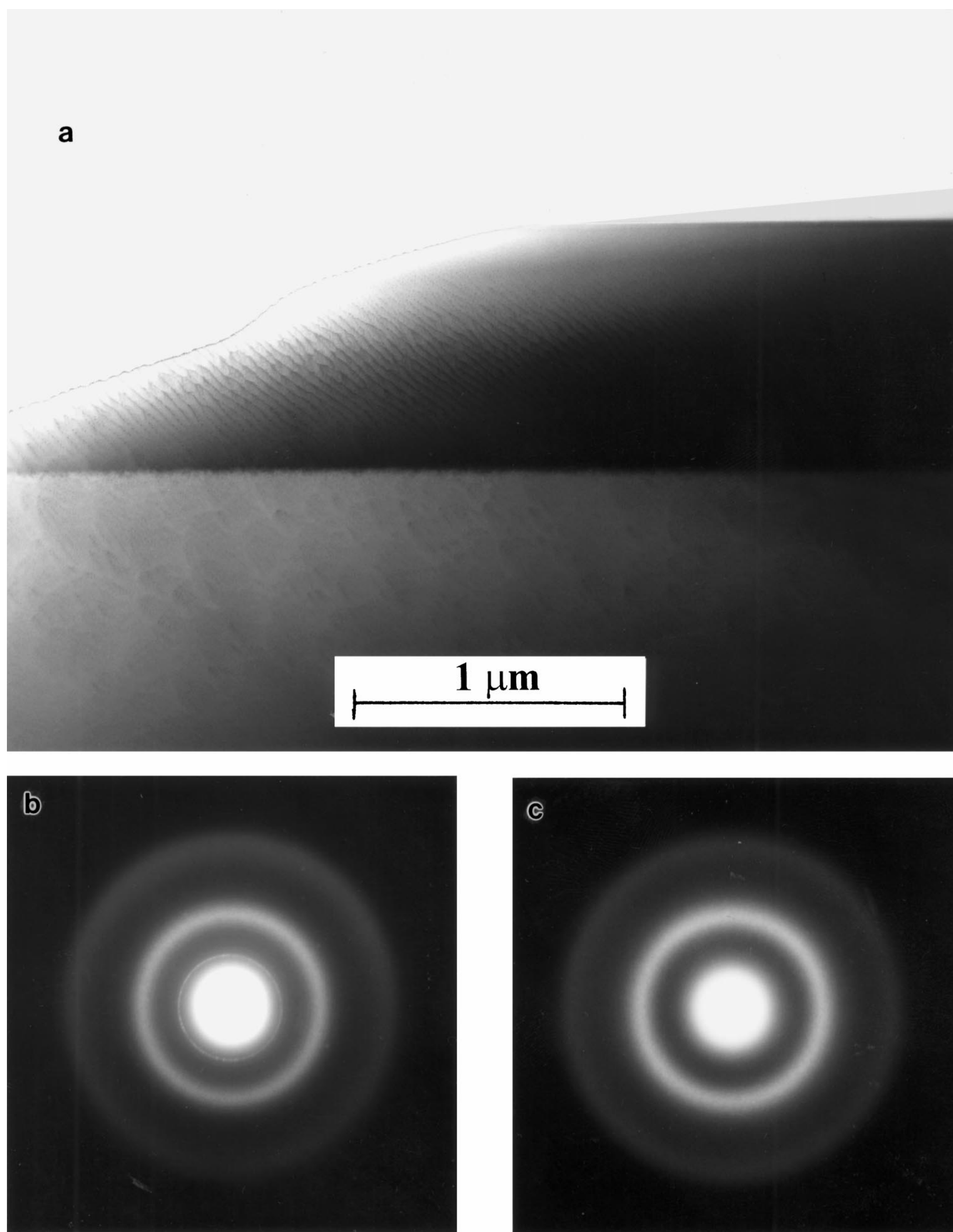

Figure 1 (a) XTEM BF image of the as-implanted sample, showing a well defined implanted layer. (b) A SADP from the as-implanted sample. Both a diffused ring due to the amorphous phase and a ring due to the crystalline Ru_2Si_3 are present. (c) A SADP from a thicker part of the implanted layer, showing only the diffuse ring.

The crystalline ring is absent in SADPs taken from the thicker parts of the implanted layer (Fig. 1c).

The amount of the Ru_2Si_3 phase in the as-implanted sample is below the detectability of XRD analysis. TEM imaging using diffraction contrast failed to reveal these ultra-fine crystallites. This suggests that the layer is largely amorphous, but contains the ultra-fine Ru_2Si_3 crystallites. The absence of the Ru_2Si_3 ring in Fig. 1c is consistent with this conclusion as the larger absorption in the thicker region tends to reduce the diffraction information from the minor phase (Ru_2Si_3). Both Rutherford back-scattered spectroscopy (RBS) and EDX mapping showed a Gaussian-like Ru depth profile.

Ion-beam-induced amorphisation is a common phenomenon for ion implantation and has been extensively studied [1]. It is well known that it is easy to amorphitise Si [1]. Thus it is not surprising to observe the amorphous layer in this work which involves high-energy implantation of heavy Ru^+ ions. We notice that some authors suggested that with increasing implantation energy the amorphous region would change from a surface layer to a submerged amorphous layer [13]. For silicon implantation into silicon, the transition between the two different microstructures occurs at an energy between 100 and 120 KeV [13, 14]. However, the present 1 MeV implantation produces a surface amorphous layer rather than the expected submerged one.

The fact that Ru_2Si_3 crystallites were formed during implantation suggests that the tendency for the formation of the silicide was remarkably high, considering that the substrate temperature during implantation was quite low (∼250°C–300°C). This can not only be explained by its large heat of formation (−60 KJ/mol.-at.) [15, 16], but also is expected by the well-known Walser and Bene's rule which predicts the first phase formation in silicon-transition metal system during low temperature solid-state reaction: the first compound nucleated in planar binary reaction couples is the most stable congruently melting compound adjacent to the lowest-temperature eutectic on the bulk equilibrium phase diagram [17]. Fig. 2 is an experimentally determined Ru-Si binary phase diagram adapted from Hashimoto [18]. From Fig. 2 it can be seen that the Si/Ru_2Si_3 eutectic transformation has the lowest temperature among the competing eutectic reactions and Ru_2Si_3 is just the congruent compound in the Ru-Si system. Thus it is not surprising to form Ru_2Si_3 during implantation.

3.2. Annealed sample

Fig. 3 is a XRD spectrum from the annealed sample, showing peaks that are attributed to polycrystalline Si and Ru_2Si_3, respectively. Fig. 4 is a TEM BF image of the annealed sample. Being consistent with the XRD result, a polycrystalline region about 660 nm thick lies on top of a single crystal Si substrate. The polycrystalline region consists of Si and Ru_2Si_3 crystals. Twin related Si grains are observed in this region (Fig. 5a). The $[110]_{Si}$ SADP from the twin related grains in Fig. 5a is shown in Fig. 5b, which is made of two variants of twins. The key to the index of Fig. 5b is shown in Fig. 5c. Extra spots are attributed to double diffraction.

Micro-area electron diffraction analysis using a fine convergent electron probe showed that small

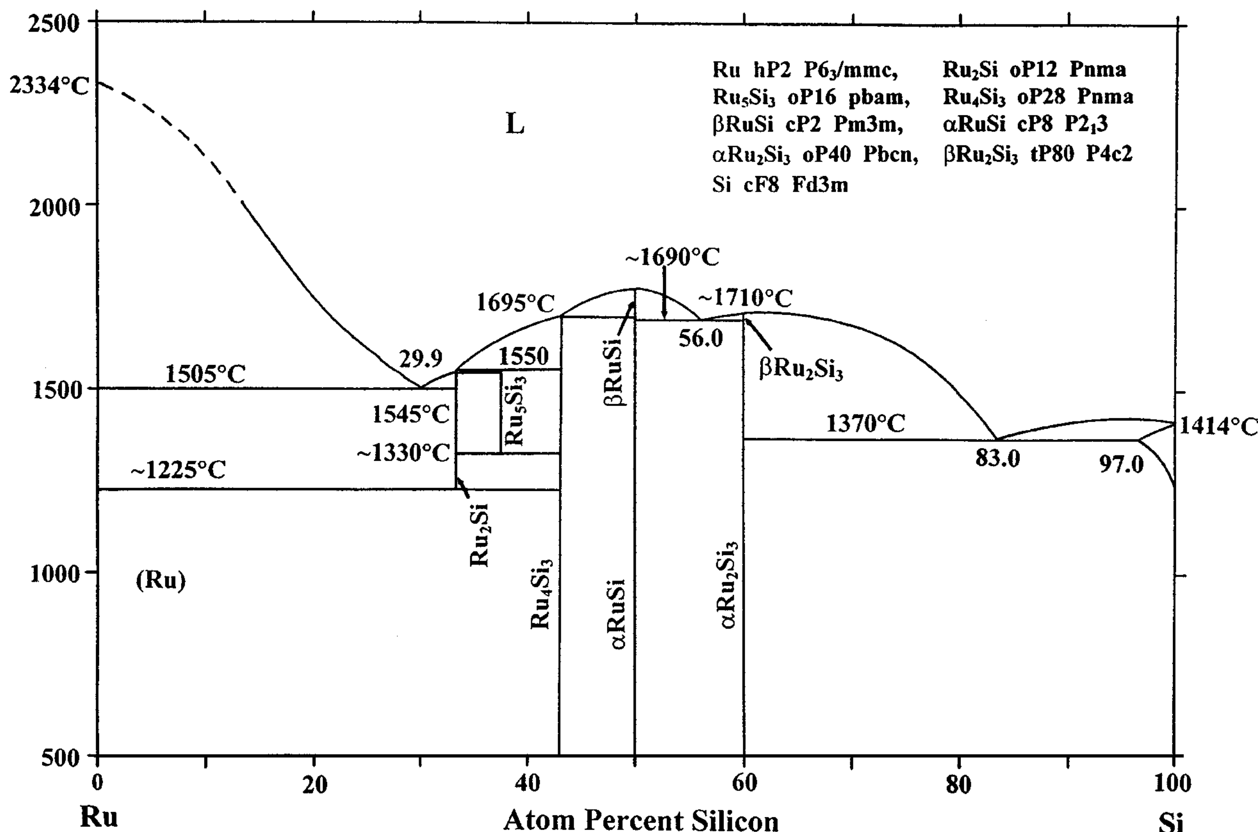

Figure 2 The Ru-Si phase diagram adapted from Hashimoto [18].

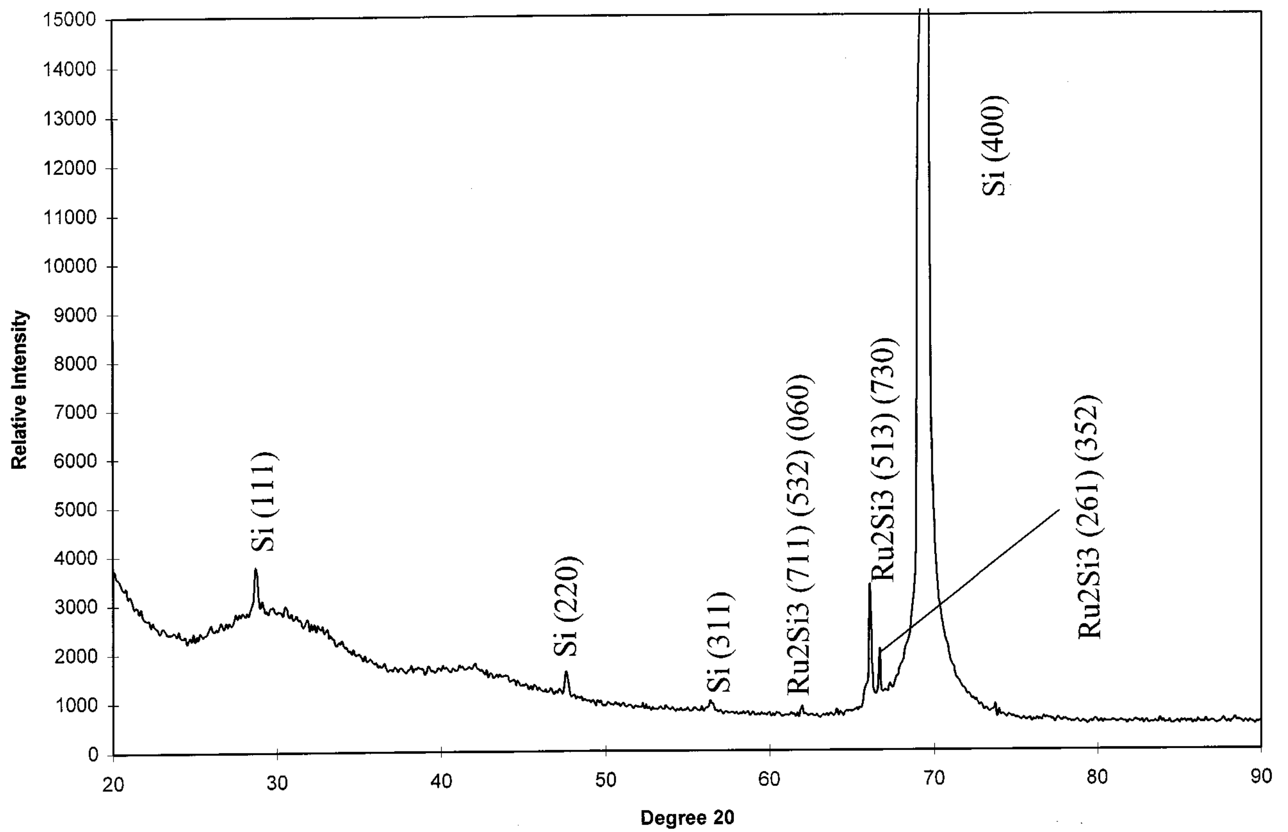

Figure 3 X-ray diffraction spectrum from the annealed sample, showing peaks due to the polycrystalline Si and Ru_2Si_3.

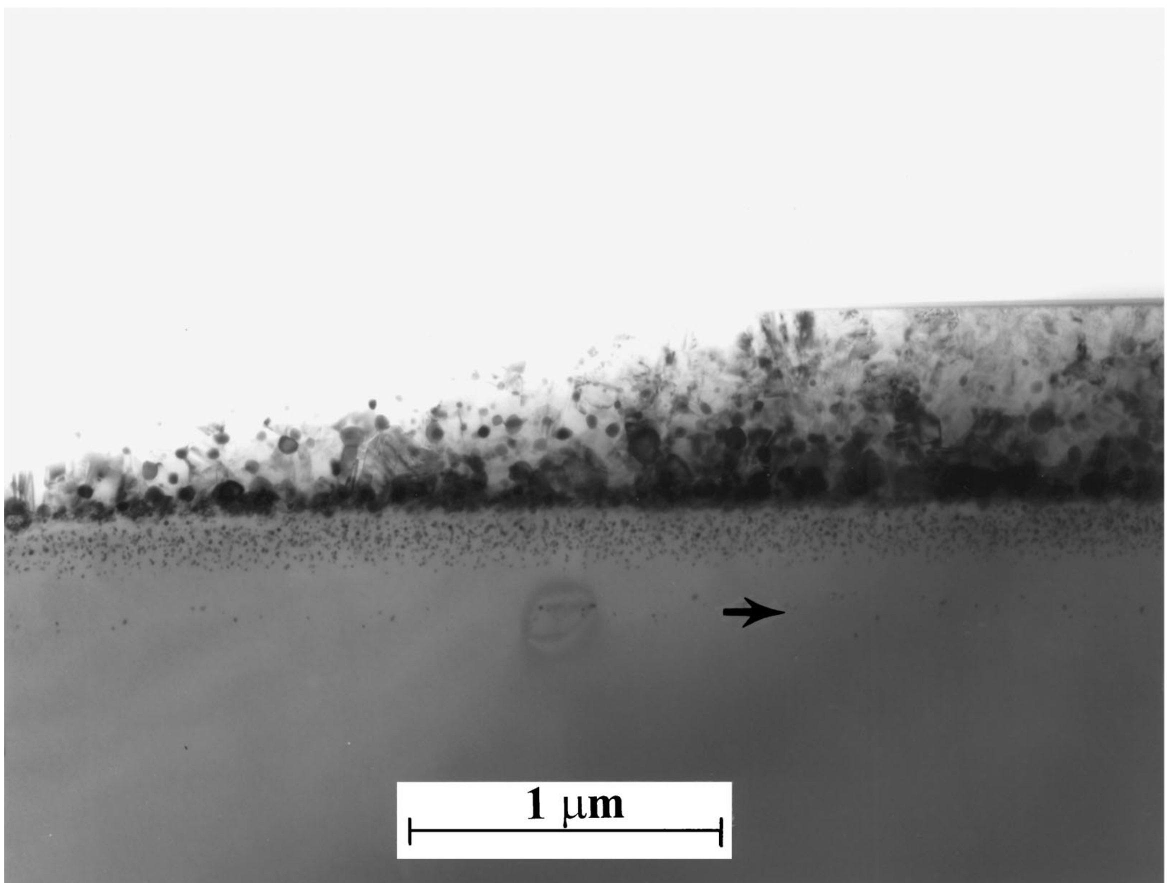

Figure 4 A XTEM BF image of the annealed sample. The arrow indicates the position of the original amorphous/crystalline interface in the as-implanted state.

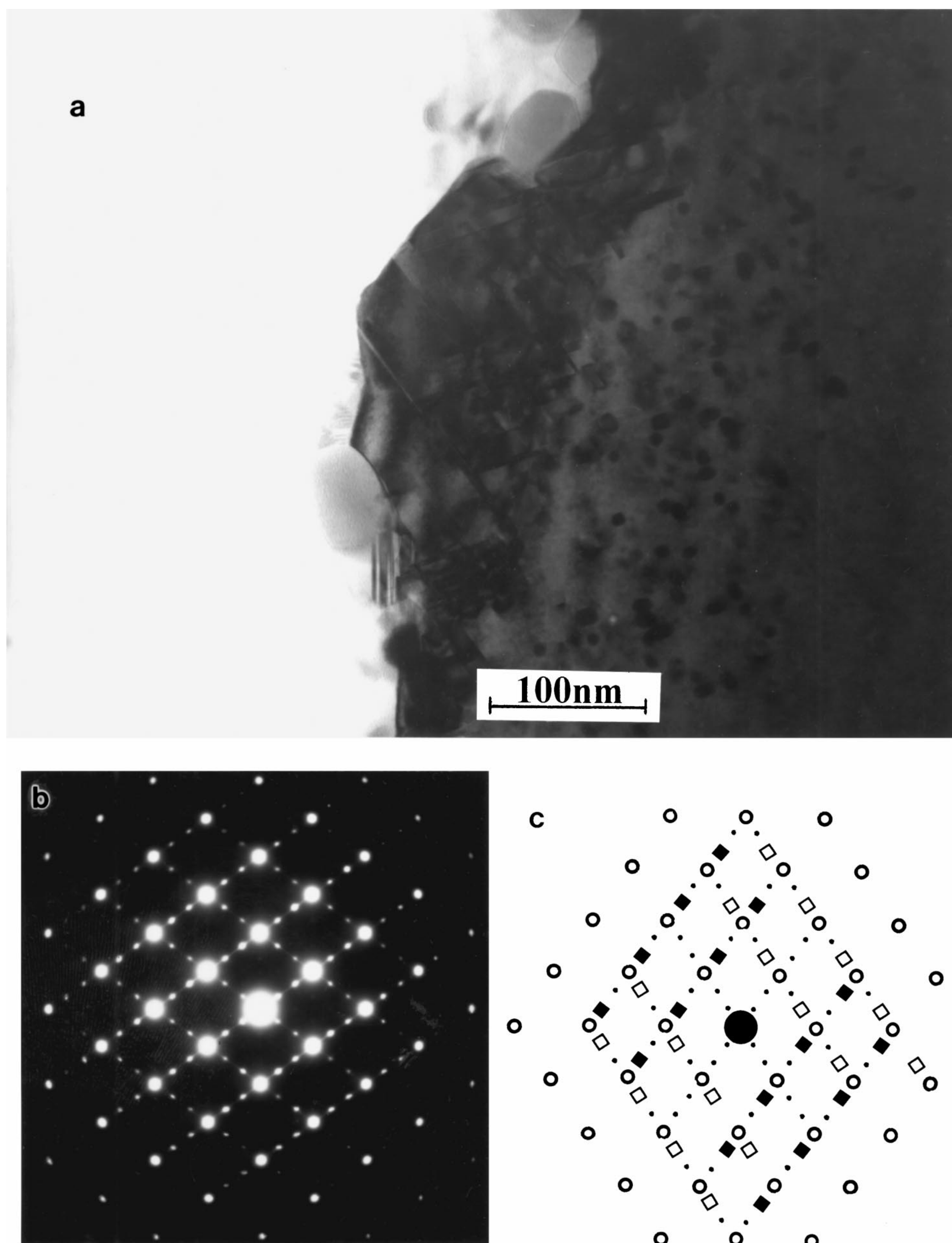

Figure 5 (a) Twin related Si grains in the polycrystalline region of Fig. 5a. (b) A SADP from the twin-related grains in (a). (c) Key to the index of (b): (◯) diffraction from matrix, (□) diffraction from twin one, (■) diffraction from twin two, (•) double diffraction.

Ru_2Si_3 grains were coexistent with polycrystalline Si grains. Fig. 6a is a [122] micro-diffraction pattern of Ru_2Si_3. The corresponding computer simulated pattern is shown in Fig. 6b. The size of the Ru_2Si_3 phase in this region is ∼40 nm.

It is necessary to point out that the polycrystalline region does not extend through the full thickness of the implanted layer. By comparing Figs 1a and 5, the position of the interface between the crystalline Si substrate and the precursor amorphous layer can be defined (indicated by an arrow in Fig. 4). The surface layer can be roughly divided into two regions, a polycrystalline region near the top surface and a region due to the advancing front of the single crystal Si substrate. The latter was formed by solid state epitaxial re-growth of the Si substrate into the precursor amorphous layer.

It was noticed that there are some very small precipitates ranging from 5 nm to 15 nm embedded in the epitaxial re-growth region, especially in the part close to the polycrystalline region. The contrast of these precipitates did not change significantly during tilting and the precipitates could always be observed. This is consistent with mass-thickness contrast due to Ru_2Si_3.

Removal of the damage caused by energetic ions has long been a main concern for the processing of thin semiconductor films. For pure Si, amorphous layers usually crystallise causing damage removal and restoration of the crystal lattice at a temperature

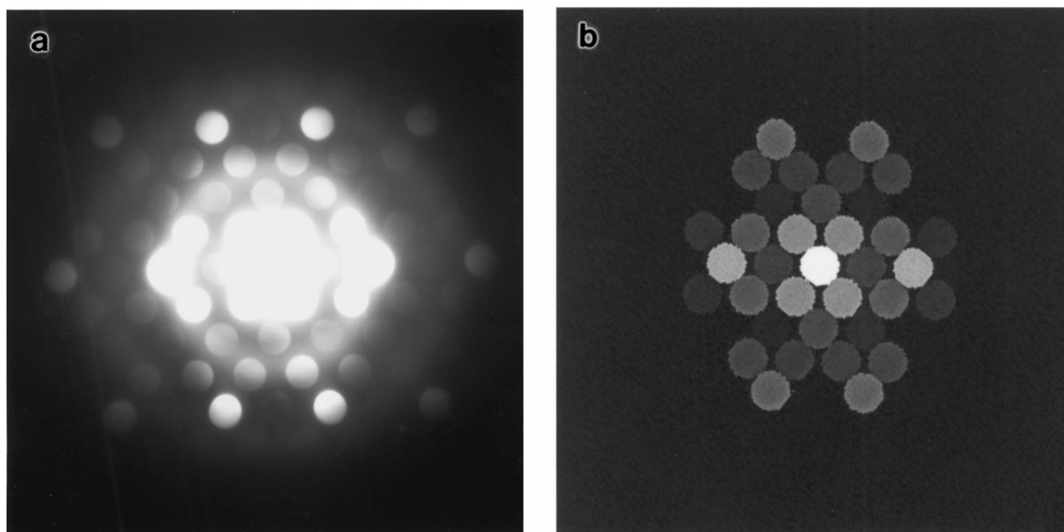

Figure 6 (a) A [122] micro-electron diffraction pattern from a small Ru_2Si_3 crystal in the polycrystalline region. (b) A computer simulated pattern corresponding to (a).

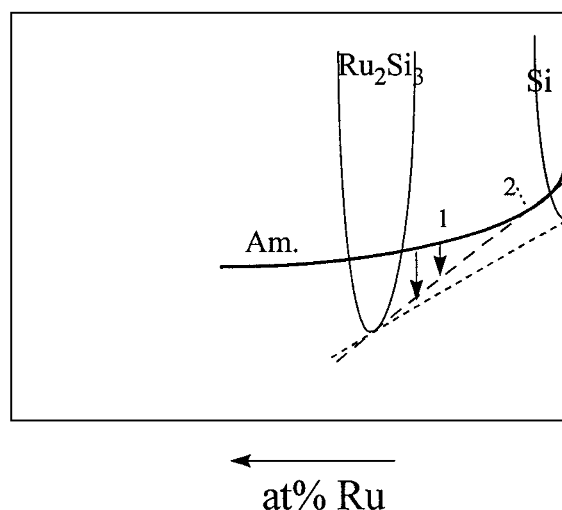

Figure 7 Schematic diagram showing hypothetical Gibbs energies of different phases. Arrows indicate the driving force for the decomposition of Am.(1) → Am.(2) + Ru_2Si_3 at different Am.(1) compositions.

around 600°C [19]. For other semiconductors, the recrystallization sequences are more complicated [1, 2]. The present results show that the Ru implantation induced amorphous layer can only fully re-crystallise via epitaxial re-growth in the region of low Ru content. This follows largely from the fact that Ru solubility in the crystalline Si is negligible below 1200°C (Fig. 2). A high Ru content in the precursor amorphous phase would not grow directly on the crystalline substrate Si via epitaxial re-growth before rejecting Ru by extensive long-range diffusion and hence nucleation and growth of the Ru_2Si_3 phase. This is demonstrated schematically in Fig. 7, which shows hypothetical Gibbs energy curves of the precursor amorphous phase and the two equilibrium product phases, i.e. the stoichiometric Ru_2Si_3 and crystalline Si phases, on the bases of the available thermodynamic data (SGTE data for pure substances [20] and standard heats of formation [15, 16] as well as the experimental phase diagram). It is seen from this figure that the amorphous phase can only decompose in two ways: (a) nucleation of Ru_2Si_3 in an amorphous matrix to allow a high Ru content in the amorphous phase, and (b) formation of crystalline Si with negligible Ru content and Ru_2Si_3. Due to the large heat of formation of the Ru_2Si_3 phase, a higher Ru content in the amorphous phase would lead to a larger driving force for its decomposition. Therefore, before the epitaxial re-growth front of Si reached the high Ru content region of the precursor amorphous layer (presumed Gaussian Ru profile), multi-nucleation of crystalline Si and Ru_2Si_3 would have occurred. The ultra-fine Ru_2Si_3 crystallites in the as-implanted precursor amorphous phase would enhance such a process via heterogeneous nucleation.

4. Conclusions

A Si wafer was implanted at high energy with ruthenium. The as-implanted sample was found to consist of an amorphous layer containing ultra-fine Ru_2Si_3 crystallites. On annealing, re-growth of the silicon substrate and further precipitation of both crystalline Si and Ru_2Si_3 occurred in the amorphous layer, leading to two different regions both containing Ru_2Si_3 nanocrystallites.

Acknowledgement

The work was partly funded by EU grant ESPRIT 28740 SILITE and the UK EPSRC grant GR/L84773. The authors also wish to thank the HEFCE for provision of the CM200 transmission electron microscope in the Microstructural Studies Unit, University of Surrey, under the Joint Research Equipment Initiative, 1997.

References

1. J. S. WILLIAMS, *Mater. Sci. & Engr.* **A253** (1998) 8.
2. H. H. TAN, J. S. WILLIAMS, J. ZOU, D. J. H. COCKAYNE, S. J. PEARTON and R. A. STALL, *Appl. Phys. Lett.* **69** (1996) 2364.
3. S. MANTL, *Nucl. Instr. and Meth.* **B80/81** (1993) 895.
4. T. D. HUNT, B. J. SEALY, K. J. REESON, R. M. GWILLIAM and K. P. HOMEWOOD, *ibid.* **B74** (1993) 60.

5. Z. YANG, G. SHAO, K. P. HOMEWOOD, K. J. REESON, M. S. FINNEY and M. HARRY, *Appl. Phys. Lett.* **67** (1995) 667.
6. D. LEONG, M. HARRY, K. J. REESON and K. P. HOMEWOOD, *Nature* **387** (1997) 686.
7. C. B. VINING, in "Thermoelectrics," edited by D. M. Rowe (CRC Press, New York, 1994) p. 227.
8. W. HENRION, M. REBIEN, V. N ANTONOV, O. JEPSEN and H. LANGE, *Thin Solid Films* **313**, **314** (1998) 218.
9. D. LENSSEN, H. L. BAY, S. MESTERS, C. DIEKER, D. GUGGI, R. CARIUS and S. MANTL, *J. Lumin.* **80** (1998) 461.
10. W. WOLF, G. BIHLMAYER and S. BLUGEL, *Phys. Rev. B* **55** (1997) 6918.
11. A. E WHITE, K. T. SHORT, R. C. DYNES, J. P. GARNO and J. M. GIBSON, *Appl. Phys. Lett.* **50** (1987) 95.
12. J. SHARPE, Y. L. CHEN, R. M. GWILLIAM, A. KEWELL, C. MCKINTY, M. LOURENÇO, G. SHAO, K. P. HOMEWOOD and K. R. KIRKBY, *ibid.* **75** (1999)1282.
13. R. E. HUMMEL, *Mater. Sci. & Engr.* **A253** (1998) 50.
14. R. E. HUMMEL, W. XI, P. H. HOLLOWAY and K. A. JONES, *J. Appl. Phys.* **63** (1988) 2591.
15. L. PERRING, P. FESCHOTTE and J. C. GACHON, *Thermochimica Acta* **293** (1997) 101.
16. S. V. MESCHEL and O. J. KLEPPA, *J. Alloys and Compounds* **274** (1998) 193.
17. R. M. WALSER and R. W. BENE, *Appl. Phys. Lett.* **28** (1976) 624.
18. H. OKAMOTO, in "ASM Handbook, Vol. 3: Alloy Phase Daigrams," edited by H. Baker, 1992. p. 2.335.
19. E. F. CSEPREGI, S. S. KENNEDY, J. W. LAU and T. W. SIGMON, *Appl. Phys. Lett.* **29** (1976) 645.
20. A. T. DINSDALE, NPL Report DAM, 195, UK National Physical Laboratory, 1989.

Received 7 February
and accepted 6 July 2000